

# Emergence of coupling-induced oscillations and broken symmetries in heterogeneously driven nonlinear reaction networks

Varsha Sreenivasan, Shakti N. Menon, and Sitabhra Sinha

*The Institute of Mathematical Sciences, CIT Campus, Taramani, Chennai 600113, India*

(Dated: March 23, 2016)

Many natural systems including the brain comprise coupled non-uniformly stimulated elements. In this paper we show that heterogeneously driven networks of excitatory-inhibitory units exhibit striking collective phenomena, including spontaneous oscillations upon coupling. On varying the coupling strength a novel transition is seen wherein the pattern symmetries of stimulated and unstimulated groups undergo mutual exchange. The system exhibits coexisting chaotic and non-chaotic attractors - an intriguing result in view of earlier reports of varying degrees of chaoticity in the brain.

PACS numbers: 05.45.Xt, 89.75.Kd, 87.19.L-

Complex patterns are observed to spontaneously emerge across a wide range of spatial and temporal scales in nature [1]. Uncovering the fundamental mechanisms driving such pattern formation will contribute significantly towards understanding self-organization in non-equilibrium systems [2]. Perhaps the most influential paradigm for explaining this, particularly in the biological context, is that of reaction-diffusion systems [3–8]. The basic principle, involving the interplay between self-activation and lateral inhibition mediated by diffusion, has been suggested to underlie the emergence of patterns in a broad range of contexts [9–12]. However, not all phenomena involving activator-inhibitor interactions arise through diffusive coupling, one of the best-known examples being populations in neighboring ecological habitats coupled through intra-specific competition [13, 14]. Indeed, reaction-diffusion processes can be seen as a subset of the wider class of systems involving nonlinear interactions between spatially distributed elements. Novel dynamical transitions may accompany the breaking of any of the symmetries that are intrinsic to these systems. Thus, uncovering the diverse range of collective phenomena associated with non-diffusively coupled systems of activator-inhibitor units can contribute towards understanding how patterns can arise in a more general setting.

Neurobiological phenomena arising in synaptically coupled neuronal populations provide some of the most varied and complex instances of nonlinear interactions resulting in spatiotemporal patterns [15]. Indeed, such coordinated collective activity is seen across several spatial scales in the brain: from the network of cortical areas where brain regions comprising  $10^3$ - $10^6$  neurons [16, 17] interact with each other through fiber tracts [18], to the olfactory bulb, where around  $10^3$  glomerular clusters coordinate the information received from sensory neurons at the nasal epithelium [19]. Each glomerulus, which comprises circuits of excitatory and inhibitory neurons, interact with other glomeruli through interneurons [20] giving rise to lateral inhibition [21] and excitation [22]. As these interneurons are subject to turnover [23], the

strength of inter-glomerular coupling can vary. Thus, this complex biological process can be potentially understood in terms of the collective dynamics of a network of excitatory-inhibitory units coupled nonlinearly with tunable strength [24]. As each glomerulus is activated by a specific odorant receptor type [25] and different smells evoke responses in different combinations of glomerular clusters [26], it is important in this context to understand the implications of non-uniform stimulation on the global behavior of such a system.

In this paper, we investigate the collective dynamics resulting from non-uniformly driven networks of identical nodes, each comprising excitatory and inhibitory subpopulations. The heterogeneous stimulation is implemented through external inputs being applied only to a subset of the nodes. This conceptual framework applies beyond the context of neurobiology to phenomena as diverse as ecological interactions between prey and predator populations [27] and interdependencies between institutions in economic systems [28, 29]. To describe the dynamics of the individual nodes, we consider a model for interacting excitatory and inhibitory subpopulations [Fig. 1 (a)] proposed by Wilson and Cowan [30] obtained by temporal coarse-graining of neuronal population dynamics. Individual units of this type are capable of exhibiting oscillatory activity for a range of external stimuli strength. In order to focus on the effect of heterogeneous stimulation, we consider the simplest connection topology, viz., coupling within and between the subpopulations of all nodes [31]. One of the novel features we observe is the occurrence of coupling-induced oscillations. Thus, stimuli that generate only steady-state behavior in isolated nodes can drive a network into oscillatory behavior, suggesting that lateral connections between glomerular clusters can allow the network to recognize weak signals incapable of initiating activity in an isolated cluster. Increasing the strength of coupling between the nodes results in a variety of transitions in the collective dynamics of the network, the most striking of which involves an exchange of symmetry between the synchronization states of the groups of stimulated and unstimulated nodes. In addi-

tion, we observe that the network can converge to qualitatively distinct attractors for identical system parameters, exhibiting chaotic or non-chaotic activity depending only on the initial state. This result is intriguing in light of observations reporting chaotic activity in the olfactory bulb, which has been suggested to have a functional role in sensory information processing [32].

We consider a network of  $N$  nodes, with each node  $i$  comprising excitatory ( $u$ ) and inhibitory ( $v$ ) components, whose activity evolves as [30]:

$$\tau_u \frac{du_i}{dt} = -u_i + (\kappa_u - r_u u_i) \mathcal{S}_u(u_i^{in}), \quad (1)$$

$$\tau_v \frac{dv_i}{dt} = -v_i + (\kappa_v - r_v v_i) \mathcal{S}_v(v_i^{in}), \quad (2)$$

where  $\tau_\mu$  are time constants ( $\mu = u, v$ ),  $u_i^{in}$  and  $v_i^{in}$  are the inputs received by the respective components,  $\mathcal{S}_\mu(x) = \kappa_\mu - 1 + [1 + \exp\{-a_\mu(x - \theta_\mu)\}]^{-1}$  is a sigmoidal response function with maximum value  $\kappa_\mu = 1 - [1 + \exp\{a_\mu\theta_\mu\}]^{-1}$ , and  $r_\mu$ ,  $a_\mu$  and  $\theta_\mu$  are system parameters. As mentioned earlier, the network is globally coupled (i.e., every node has  $k = N - 1$  links) with each link having the same weight  $w/k$ . This normalization allows our results to be system-size independent. The total inputs to each component of node  $i$  are  $u_i^{in} = c_{uu}u_i - c_{uv}v_i + \frac{w}{k} \sum_j (u_j - v_j) + I_{u_i}$  and  $v_i^{in} = c_{vu}u_i - c_{vv}v_i + \frac{w}{k} \sum_j (u_j - v_j) + I_{v_i}$ , where  $j = 1, \dots, N$  ( $j \neq i$ ). To implement heterogeneous stimulation different external inputs ( $I_{u_i}$ ,  $I_{v_i}$ ) can be applied to different nodes. For the results shown here we have used the following set of parameter values:  $c_{uu}=16$ ,  $c_{uv}=15$ ,  $c_{vu}=12$ ,  $c_{vv}=3$ ,  $a_u=1.3$ ,  $a_v=2$ ,  $\theta_u=4$ ,  $\theta_v=3.7$ ,  $r_{u,v}=1$ ,  $\tau_{u,v}=8$  and  $I_v = 0$ . We have verified that our results are robust with respect to changes in these parameter values.

On receiving a stimulus  $I_u$  of sufficient magnitude, a single node is capable of exhibiting limit-cycle oscillations around an unstable fixed point [30] [Fig. 1 (b)]. This limit cycle emerges via the collision of stable and saddle branches [Fig. 1 (c)], and the amplitude of oscillation depends on the value of  $I_u$  [Fig. 1 (d)]. As shown in Fig. 1 (e) and discussed in detail in Ref. [31], coupling identically stimulated nodes yields a rich variety of synchronization patterns including exact synchronization (ES), quasiperiodicity (QP), anti-phase synchronization (APS) and inhomogeneous in-phase synchronization (IIS) at different  $w$  and  $I_u$ .

In this work, we consider heterogeneously driven networks wherein the number of nodes receiving external stimulus  $N_{stim} < N$ . We henceforth denote the synchronization state in such systems through the notation  $(P_{stim}, P_{unstim})$ , where the first and second terms in the pair correspond to the collective pattern observed in the stimulated and unstimulated nodes, respectively. The simplest case of non-uniform stimulation is when a single node receiving input  $I_u$  is coupled to an unstimulated node (i.e.,  $N = 2$ ,  $N_{stim} = 1$ ) with strength  $w$ . At suf-

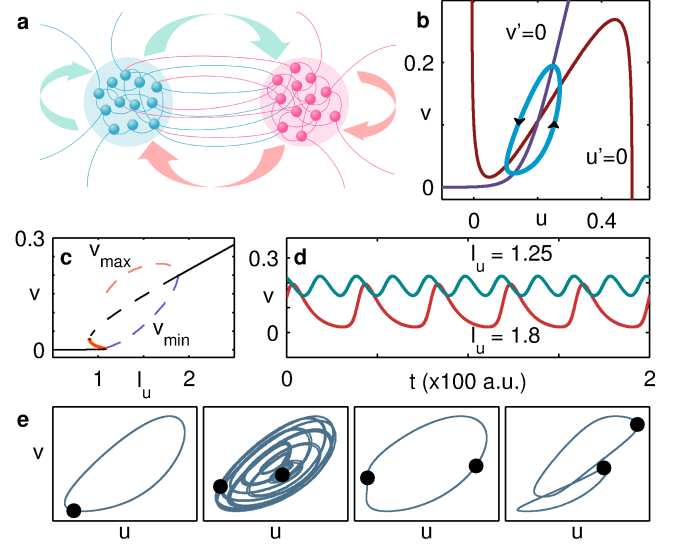


FIG. 1. (a) Schematic representation of a dynamical element (node) of the network, showing the interactions between sub-populations of excitatory and inhibitory units (neurons). (b) Nullclines governing the dynamics of a node receiving stimulus  $I_u = 1.25$  along with the resulting limit cycle attractor. (c) Bifurcation diagram for the inhibitory component  $v$  of an isolated node shown as a function of the stimulus  $I_u$ . The broken lines indicate the unstable branch (black), as well as the peaks ( $v_{max}$ , pink) and troughs ( $v_{min}$ , violet) in the oscillatory regime. The solid black and thick red curves indicate the stable and saddle branches, respectively. (d) The  $v$  time-series of an isolated node receiving stimuli  $I_u = 1.25$  (green) and  $I_u = 1.8$  (red). (e) Phase-plane portraits for a pair of identically stimulated coupled nodes (i.e.,  $N_{stim} = N = 2$ ) for different  $w$  and  $I_u$  showing [L-R] exact synchronization (ES), quasiperiodicity (QP), anti-phase synchronization (APS) and inhomogeneous in-phase synchronization (IIS). The positions of the oscillators are denoted by black filled circles.

ficiently large  $w$ , oscillations can be observed even for very low  $I_u$  [Fig. 2 (a)]. Indeed, as shown in the phase diagram in Fig. 2 (b), at high  $w$  periodic activity can be observed over a much larger range of  $I_u$  than the one capable of inducing oscillations in an isolated node. Furthermore, for lower (higher)  $w$  the unstimulated node has lower (higher) amplitude oscillations than the stimulated one, denoted as OSC1 (OSC2). This extremely surprising *coupling-induced periodic activity* is seen even when  $N \gg N_{stim} = 1$  (see Supplementary Information) and suggests that a node is capable of detecting weak, subthreshold inputs when it is coupled to one or more unstimulated nodes. Such an increase in the sensitivity to stimuli beyond the capability of a single element is an emergent collective property of the network and may be understood as an effective renormalization of the parameters governing the nodal dynamics. The observation of oscillations at larger values of  $I_u$ , where an isolated node exhibits a stable state, may also be connected to the appearance of periodic activity in bistable systems,

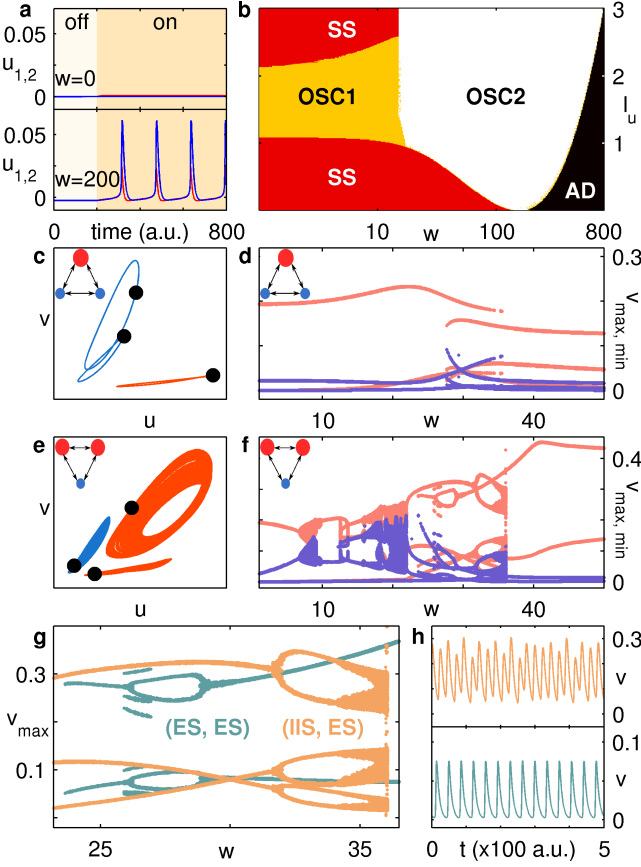


FIG. 2. (a-b) Coupling-induced oscillations in a pair of nodes, where only one receives a stimulus  $I_u$ . (a) By switching “on” a stimulus that is too weak ( $= 0.1$ ) to generate activity in the uncoupled nodes (top), oscillations can be observed by strongly coupling the stimulated (red) and unstimulated (blue) nodes (bottom). (b) The range of  $I_u$  for which oscillations emerge increases at higher  $w$ . The amplitude of the oscillations is larger for the stimulated node at low  $w$  (OSC1) and for the unstimulated node at high  $w$  (OSC2). The other dynamical regimes observed correspond to a non-zero steady state (SS) and a quiescent state characterizing amplitude death (AD). The regimes are determined via order parameters and identified as the pattern obtained from the majority ( $> 50\%$ ) of random initial states (see Supplementary Information). (c-h) Symmetry breaking in a system of  $N = 3$  globally coupled nodes. The stimulated (large, red) and unstimulated (small, blue) nodes are indicated schematically in top-left corner of (c-f). Phase space projections of the trajectories (colored as per the schematic) are shown for (c)  $N_{\text{stim}} = 1$ , displaying (ES, IIS) state (note the broken symmetry in unstimulated nodes) and (e)  $N_{\text{stim}} = 2$ , exhibiting chaos. In the corresponding bifurcation diagrams for (d)  $N_{\text{stim}} = 1$  and (f)  $N_{\text{stim}} = 2$ , the peaks ( $v_{\text{max}}$ , pink) and troughs ( $v_{\text{min}}$ , violet) of the inhibitory component are shown as a function of  $w$ . (g) Magnified view of (f) showing the coexistence of qualitatively distinct dynamical attractors corresponding to (IIS, ES) [orange] and (ES, ES) [green]. The system can exhibit either chaotic or non-chaotic behavior depending on its initial state, as illustrated in the top and bottom panels of (h) for  $w = 35.6$ .

e.g., excitable elements subjected to a sufficiently strong stimulus, upon appropriate coupling [33]. On increasing  $w$  beyond a critical value that depends on the stimulus intensity  $I_u$ , the activity of all nodes ceases, which corresponds to a state of amplitude death (AD).

A new feature, indicative of *spontaneous symmetry breaking*, appears on minimally increasing the size of the network to  $N = 3$  keeping  $N_{\text{stim}} = 1$ . This is manifested as IIS in the unstimulated nodes [Fig. 2 (c)], neither of which directly receive any external stimuli but are activated only by coupling with a common stimulated node. Nevertheless these identical nodes exhibit distinct oscillation patterns over a range of coupling strengths [Fig. 2 (d)]. On stimulating a second node (i.e.,  $N = 3$ ,  $N_{\text{stim}} = 2$ ), another intriguing phenomenon emerges, viz., the *coexistence* of chaotic and non-chaotic attractors. The existence of chaotic behavior [Fig. 2 (e)], which arises via a period doubling route [Fig. 2 (f)] is confirmed by verifying the existence of positive Lyapunov exponents [34]. Note that if we use a smaller  $I_u$ , chaos can be seen in the even simpler stimulation configuration  $N_{\text{stim}} = 1$ ,  $N = 3$ . The novel feature for  $N_{\text{stim}} = 2$  is that, depending on initial conditions, it is possible to see either of two possible collective dynamical states corresponding to (ES, ES) or (IIS, ES), the latter being a chaotic attractor. As both the (IIS, ES) and (ES, ES) states have non-zero basin sizes [Fig. 2 (g)] we can see either chaotic or non-chaotic behavior for identical system parameters over a range of  $w$  [Fig. 2 (h)]. This observation lends support to the hypothesis, based on experimental recordings from the rabbit olfactory system, that attractors with varying degrees of chaoticity can coexist in the brain [35].

The existence of numerous synchronization regimes in the  $w - N_{\text{stim}}$  parameter space becomes apparent as we increase the complexity of the system by incorporating more nodes [Fig. 3 (a)]. These regimes are typically demarcated by sharp changes in the sizes of the basin of attraction of individual patterns indicated in Fig. 3 (b-c). Apart from the states corresponding to ES, QP, IIS and AD described earlier, new collective dynamical patterns for the stimulated and unstimulated groups emerge. These include oscillator death (OD) which is a homogeneous non-zero steady state, and gradient synchronization (GS), a generalization of APS for systems with  $N > 2$  [31]. Fig. 3 (d) shows several of the possible collective patterns, including those corresponding to symmetry breaking (IIS) in one or both groups of stimulated and unstimulated nodes. A particularly surprising feature that we investigate in detail below is the existence of a novel transition in which the (broken) symmetry of the patterns in the stimulated and unstimulated groups undergo a mutual exchange on varying the coupling strength. This symmetry exchange manifests as a transition from the (IIS, ES) to the (ES, IIS) state [Fig. 3 (a)].

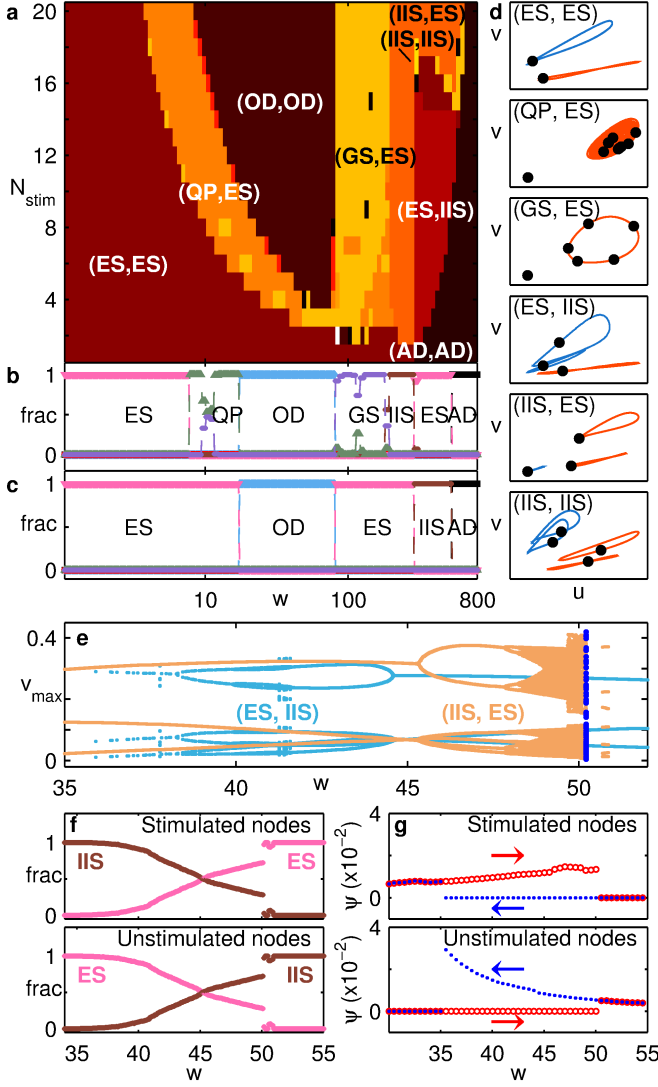


FIG. 3. (a-d) Collective dynamics of a system of  $N = 20$  globally coupled nodes. (a) Different synchronization states obtained by varying the number of stimulated nodes,  $N_{\text{stim}}$ , and coupling strength,  $w$ , with  $(P_{\text{stim}}, P_{\text{unstim}})$  referring to patterns in stimulated and unstimulated groups. (b-c) Variation of the attraction basin size (measured as fraction of initial states reaching the attractor) with  $w$  at  $N_{\text{stim}} = 10$  for the different regimes in (a), shown separately for the (b) stimulated and (c) unstimulated groups. Basin sizes have been estimated using  $10^2$  initial conditions. (d) Phase space projections of the trajectories (red: stimulated, blue: unstimulated) corresponding to the different synchronization states indicated in (a). (e-g) Symmetry exchange transition in a system of  $N = 4$  globally coupled oscillators with  $N_{\text{stim}} = 2$ . (e) Bifurcation diagram showing the peaks ( $v_{\text{max}}$ ) of the inhibitory components of all nodes as  $w$  is varied. Distinct coexisting attractors corresponding to (IIS, ES) and (ES, IIS) are indicated by orange and light blue, respectively. (f-g) Variation of the (f) fractional basin size of these attractors and (g) the order parameter  $\psi = \langle \sigma_i^2(v_i) \rangle$  with  $w$ , shown separately for the (top) stimulated and (bottom) unstimulated groups. The distinct trends seen in (g) on increasing (red circle) or decreasing (blue dots)  $w$  indicate the occurrence of hysteresis-like behavior.

We examine the nature of this transition in detail by considering the simplest system in which it can be observed. To observe broken symmetry in each group, both the stimulated and unstimulated groups should contain at least two nodes each. We observe that in the minimal case, i.e., for  $N = 4$ ,  $N_{\text{stim}} = 2$ , the states (IIS, ES) and (ES, IIS) co-exist over a range of  $w$  [Fig. 3 (e)]. The transition between them occurs through a change in the relative basin sizes for the patterns in the two groups [Fig. 3 (f)]. The mechanism of the (broken) symmetry exchange is further established by examining how the order parameter  $\psi = \langle \sigma_i^2(v_i) \rangle$  (non-zero values of which indicate IIS in this regime) changes upon varying  $w$  in either direction in an annealed manner. In this procedure, the system is allowed to evolve starting from a random initial state at low (high)  $w$ , following which the value of  $w$  is adiabatically increased (decreased). As seen in Fig. 3 (g), a hysteresis-like behavior can be observed in the transition region in both groups of nodes, consistent with the mechanism of shrinking basin sizes underlying the symmetry exchange.

Our results provide a simple framework for understanding aspects of the complex patterns of spatiotemporal activity that the brain is observed to exhibit [36]. The mesoscopic approach used here, focusing on the dynamics of a network of neuronal clusters, can yield significant insights into the mechanisms by which such patterns emerge. Furthermore, the phenomena we report here occurs in a globally connected system, which may help elucidate the important role of long-range intracortical interactions in olfactory processing [37]. Among the variety of dynamical transitions observed upon varying the coupling strength, the most striking one involves an exchange of broken and restored symmetries between the groups of stimulated and unstimulated nodes. This result suggests an experimentally testable hypothesis, namely that simulated and non-stimulated glomeruli may show distinct collective dynamics at different levels of arousal which are analogous to having different coupling strengths between nodes.

To conclude, we have shown that non-uniformly driven networks of identical nodes, each comprising excitatory and inhibitory subpopulations, are capable of exhibiting surprisingly rich collective phenomena. We find that the system exhibits *coexistence of qualitatively distinct attractors* (chaotic and non-chaotic) for identical system parameters. This is intriguing in light of experimental observations of chaotic dynamics of varying complexity, particularly in the olfactory system [32, 35, 38], reported over several decades and which are yet to be fully understood. Furthermore, nodes that are quiescent in isolation can spontaneously oscillate for sufficiently strong coupling, thus enabling the system to be activated even by stimuli that are incapable of generating dynamical activity in isolated nodes. These *coupling-induced oscillations* may help in understanding how excitatory-

inhibitory feedback can cause spontaneous oscillations in networks of naturally quiescent stochastic spiking neurons [39], whose mean-field limit can in fact be described through the Wilson-Cowan equations. Moreover, this can be understood as belonging to a larger class of phenomena characterized by the emergence of activity in quiescent systems upon coupling [40–42]. In summary, our results suggest that transitions between symmetry broken and restored symmetry states in heterogeneously driven system of coupled neural oscillators may underlie the sequence of complex activity patterns seen in the brain.

We would like to thank Bhaskar Saha, Rajeev Singh, Sudeshna Sinha, Deepak Dhar and K. A. Chandrashekar for helpful discussions. SNM is supported by the IMSc Complex Systems Project (12<sup>th</sup> Plan). VS is supported by the ITRA Project. We thank IMSc for providing access to the supercomputing cluster “Satpura”, which is partially funded by DST.

- 
- [1] P. Ball, *The Self-Made Tapestry: Pattern Formation in Nature* (Oxford University Press, Oxford, 1999).
  - [2] M. C. Cross and P. C. Hohenberg, *Rev. Mod. Phys.* **65**, 851 (1993).
  - [3] J. D. Murray, *Sci. Am.* **258**, 80 (1988).
  - [4] A. J. Koch and H. Meinhardt, *Rev. Mod. Phys.* **66**, 1481 (1994).
  - [5] M. Tlidi, P. Mandel, and R. Lefever, *Phys. Rev. Lett.* **73**, 640 (1994).
  - [6] S. Kondo and T. Miura, *Science* **329**, 1616 (2010).
  - [7] T. Bánsági, V. K. Vanag, and I. R. Epstein, *Science* **331**, 1309 (2011).
  - [8] R. Kapral, and K. Showalter, *Chemical Waves and Patterns* (Springer, New York, 2012).
  - [9] A. De Wit, D. Lima, G. Dewel, and P. Borckmans, *Phys. Rev. E* **54**, 261 (1996).
  - [10] V. K. Vanag and I. R. Epstein, *Phys. Rev. Lett.* **92**, 128301 (2004).
  - [11] H. Nakao and A. S. Mikhailov, *Nat. Phys.* **6**, 544 (2010).
  - [12] R. Singh and S. Sinha, *Phys. Rev. E* **87**, 012907 (2013).
  - [13] M. E. Gilpin and F. J. Ayala, *Proc. Natl. Acad. Sci. USA* **70**, 3590 (1973).
  - [14] H. I. Wu, P. J. Sharpe, J. Walker, and L. K. Penridge, *Ecological Modelling* **29**, 215 (1985).
  - [15] K. J. Friston, *Phil. Trans. Roy. Soc. B* **355**, 215 (2000).
  - [16] G. Palm, *Hippocampus* **3**, 219 (1993).
  - [17] C. Johansson and A. Lansner, *Neural Netw.* **20**, 48 (2007).
  - [18] D. S. Modha and R. Singh, *Proc. Natl. Acad. Sci. USA* **107**, 13485 (2010).
  - [19] P. Mombaerts, F. Wang, C. Dulac, S. K. Chao, A. Nemes, M. Mendelsohn, J. Edmondson, and R. Axel, *Cell* **87**, 675 (1996).
  - [20] G. Lowe, Olfactory bulb: Synaptic organization. *In: Encyclopedia of Life Sciences* (John Wiley & Sons, Ltd, Chichester, 2013).
  - [21] T. Imai, *Semin. Cell Dev. Biol.* **35**, 180 (2014).
  - [22] J. M. Christie and G. L. Westbrook, *J. Neurosci.* **26**, 2269 (2006).
  - [23] P. M. Lledo, F. T. Merkle, and A. Alvarez-Buylla, *Trends. Neurosci.* **31**, 392 (2008).
  - [24] M. Migliore, F. Cavarretta, A. Marasco, E. Tulumello, M. L. Hines, and G. M. Shepherd, *Proc. Nat. Acad. Sci. USA* **112**, 8499 (2015).
  - [25] P. Mombaerts, *Annu. Rev. Cell Dev. Biol.* **22**, 713 (2006).
  - [26] B. Malnic, J. Hirono, T. Sato, and L. B. Buck, *Cell* **96**, 713 (1999).
  - [27] R. M. May and A. R. McLean, *Theoretical Ecology: Principles and Applications* (Oxford University Press, Oxford, 2007).
  - [28] R. M. May, S. A. Levin, and G. Sugihara, *Nature* **451**, 893 (2008).
  - [29] F. Schweitzer *et al.*, *Science* **325**, 422 (2009).
  - [30] H. R. Wilson and J. D. Cowan, *Biophys. J.* **12**, 1 (1972).
  - [31] R. Singh, S. N. Menon, and S. Sinha, *Sci. Rep.* **6**, 22074 (2016).
  - [32] W. J. Freeman, *Sci. Am.* **264**, 78 (1991).
  - [33] V. In, A. R. Bulsara, A. Palacios, P. Longhini, A. Kho, and J. D. Neff, *Phys. Rev. E* **68**, 045102 (2003).
  - [34] A. Wolf, J. B. Swift, H. Swinney, and J. A. Vastano, *Physica D* **16**, 285 (1985).
  - [35] W. J. Freeman, *How Brains Make Up Their Minds*. (Columbia University Press, New York, 2000).
  - [36] R. I. Wilson and Z. F. Mainen, *Annu. Rev. Neurosci.* **29**, 163 (2006).
  - [37] M. Luo, *Neuron* **72**, 1 (2011).
  - [38] H. Korn and P. Faure, *C. R. Biologies* **326**, 787 (2003).
  - [39] E. Wallace, M. Benayoun, D. W. Van, and J. D. Cowan, *PLoS One* **6**, e14804 (2011).
  - [40] A. F. Taylor, M. R. Tinsley, F. Wang, Z. Huang, and K. Showalter, *Science* **323**, 614 (2009).
  - [41] R. Singh, J. Xu, N. G. Garnier, A. Pumir, and S. Sinha, *Phys. Rev. Lett.* **108**, 068102 (2012).
  - [42] J. Xu, S. N. Menon, R. Singh, N. B. Garnier, S. Sinha, and A. Pumir, *PLoS One* **10**, e0118443 (2015).

## SUPPLEMENTARY INFORMATION

### ORDER PARAMETERS

The identification of each collective dynamical state is done by measuring a set of order parameters and then using the decision tree in Fig. S1 to classify the synchronization state. The same procedure is applied independently for the stimulated and the unstimulated groups of nodes. At each numbered decision point, threshold values (Table S1) for the order parameters are employed to answer the following questions:

1. Whether the magnitude of the inhibitory component of each oscillator changes over time. For a non-oscillating state, this quantity should be below a threshold  $\varepsilon_0$ .
2. Whether the magnitude of the inhibitory component of each oscillator is close to zero for all oscillators. If this quantity is below a threshold  $\varepsilon_1$ , it signifies amplitude death.
3. Whether the temporal mean of each oscillator is the same. If the difference is below a threshold  $\varepsilon_2$ , it signifies oscillator death; otherwise it is an inhomogeneous steady state.
4. Whether all the oscillators are in phase. If the difference between the phases of the oscillators is less than a threshold  $\varepsilon_3$ , it corresponds to exact synchronization.
5. Whether the temporal mean of each oscillator is the same. If the difference is greater than a threshold  $\varepsilon_4$ , it signifies inhomogeneous in-phase synchronization. In the oscillating case, once phase synchronization has been established, this order parameter checks if all oscillators have the same trajectory.
6. Whether the total amount of phase space covered by the trajectory is small. For the case of GS, this quantity is less than a threshold  $\varepsilon_5$ ; if the quantity is greater than the threshold, the state is identified as QP which, by definition, completely fills a bounded region in phase space.

Threshold	Value (Stimulated)	Value (Unstimulated)
$\varepsilon_0$	$10^{-7}$	$10^{-15}$
$\varepsilon_1$	$10^{-10}$	$10^{-10}$
$\varepsilon_2$	$10^{-10}$	$10^{-15}$
$\varepsilon_3$	$10^{-9}$	$10^{-12}$
$\varepsilon_4$	$10^{-4}$	$10^{-5}$
$\varepsilon_5$	$2 \times 10^4$	$2 \times 10^4$

TABLE S1. Thresholds for the order parameters used to distinguish the synchronization patterns (see Fig. S1). To account for the fact that unstimulated nodes typically exhibit much smaller oscillations, the chosen threshold values are in general different for the stimulated and the unstimulated groups.



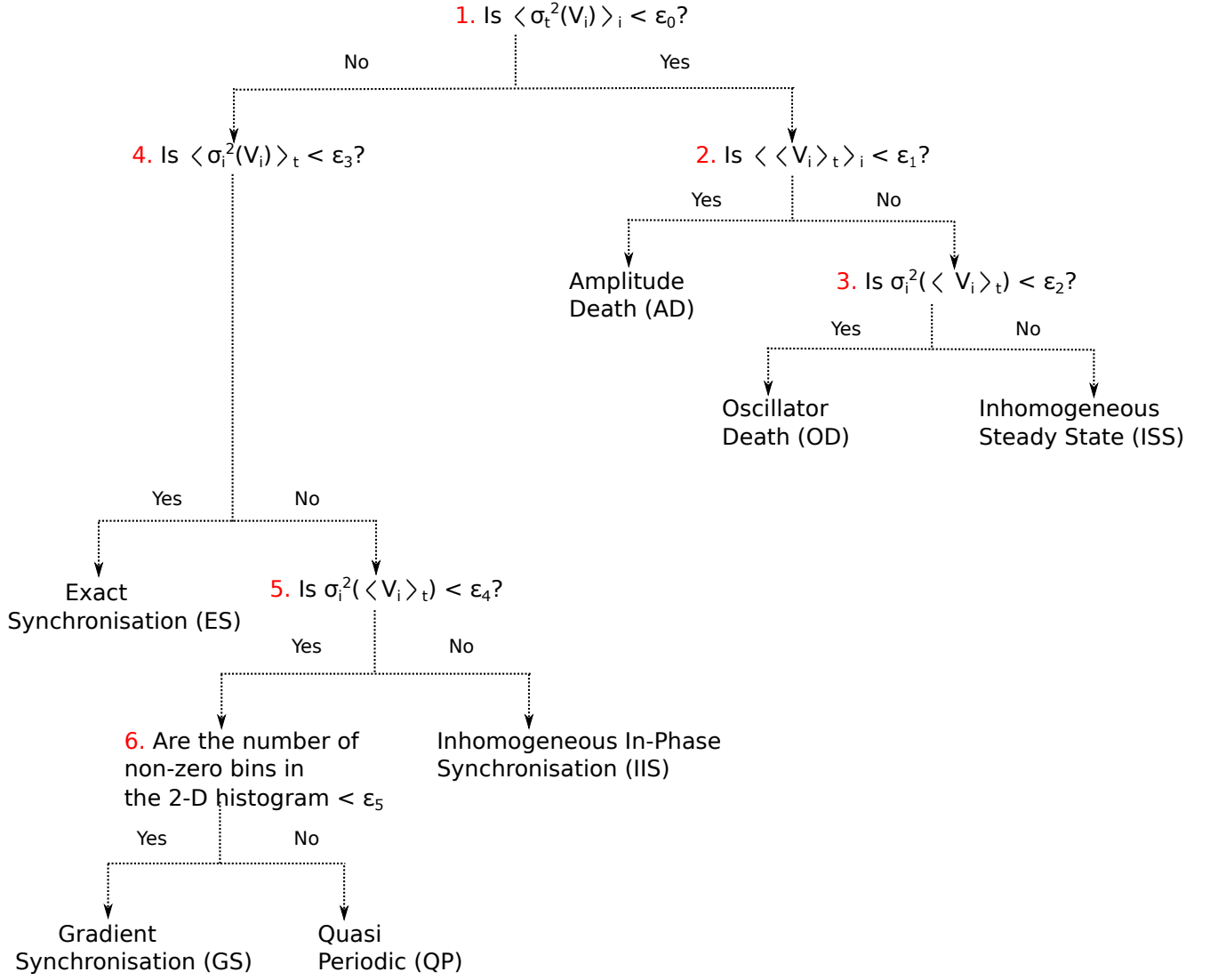


FIG. S1. Decision tree for the use of order parameters to distinguish between the different collective dynamical states. Although this tree is identical for both stimulated and unstimulated oscillators, the threshold values chosen for identifying the corresponding patterns are different (see Table S1).

## ROBUSTNESS OF RESULTS

In the following, we demonstrate that the results presented in the main text are robust with respect to small changes in the system parameters or system size. First, we consider the case of coupling-induced oscillations, shown in Fig. 2 (a) of the main text. As seen in Fig. S2, steady state behavior is exhibited by a globally coupled system of  $N$  ( $= 3, 5$ ) nodes, with only  $N_{\text{stim}} = 1$  of them receiving a weak input stimulus  $I_u$ . Although the stimulation is too weak to initiate activity in an isolated node, upon coupling these nodes with sufficient strength  $w$ , we find that oscillations emerge, as in the case  $N = 2$  considered in the main text.

Next, we consider the symmetry switching transition discussed in the main text. In Fig. 3 (e) of the main text, we see that for the case  $N = 4$ ,  $N_{\text{stim}} = 2$  there exists a range of values within which the distinct collective dynamical states (ES, IIS) and (IIS, ES) coexist. As seen in Fig. 3 (f), the likelihood of obtaining the pattern pair (IIS, ES) is higher at lower values of coupling strength  $w$ , and only (ES, IIS) is obtained above a critical value of  $w$ . These results hold even for much larger system sizes, as shown in Fig. S3, which displays a bifurcation diagram for the case  $N = 20$ ,  $N_{\text{stim}} = 10$ . As we can see, the pattern pair (IIS, ES) is seen for lower  $w$ , and (ES, IIS) is seen for higher  $w$ .

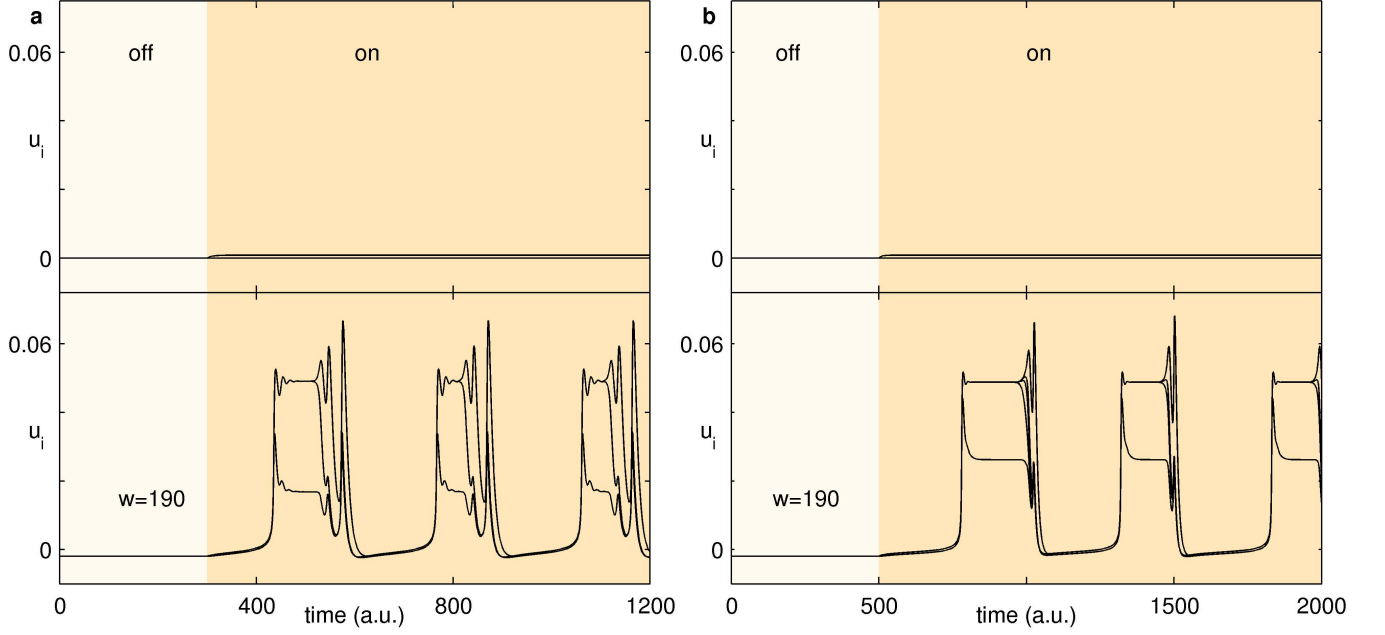


FIG. S2. Coupling-induced oscillations in a system of (a)  $N = 3$  and (b)  $N = 5$  nodes, where only one node receives a stimulus  $I_u = 0.1$  that is too weak to generate activity in the uncoupled nodes (top). Oscillations can be observed by strongly coupling ( $w = 190$ ) the nodes (bottom).

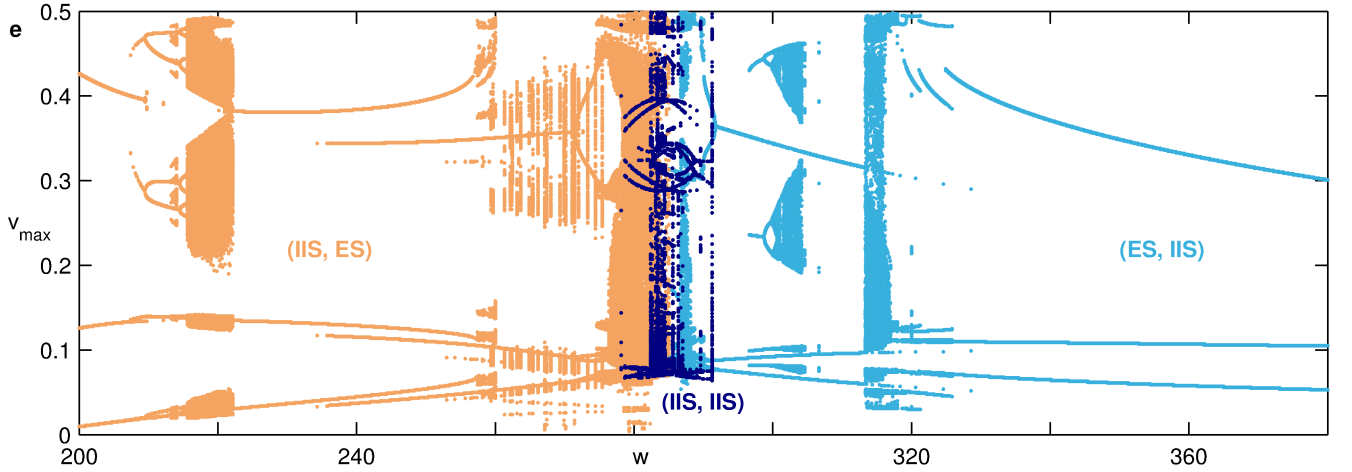


FIG. S3. Bifurcation diagram for a network with  $N = 20$ ,  $N_{\text{stim}} = 10$ , with the peaks ( $v_{\text{max}}$ ) of the inhibitory component,  $v$ , indicated over a range of  $w$ . Colors are used to represent different collective dynamical states, viz., orange for (IIS, ES), light blue for (ES, IIS) and dark blue for (IIS, IIS). On increasing  $w$ , a transition occurs from (IIS, ES) to (ES, IIS), corresponding to an exchange of (broken) symmetries between the stimulated and unstimulated groups.

Finally, we show that our results are robust with respect to changes in both the internal coupling parameters as well as the input stimulus applied to the inhibitory components ( $I_v$ ). In Fig. S4 (a), we show a parameter space diagram indicating the synchronization states obtained upon changing  $w$  as well as the ratio  $I_v/I_u$ , for the case  $N = 4$ ,  $N_{\text{stim}} = 2$ . Note that, for these simulations, the values of all the internal coupling strengths  $c_{\mu,\nu}$  have been halved relative to those used for the simulations reported in the main text. We find that for low values of the ratio ( $\lesssim 0.25$ ) the patterns observed, and their phase boundaries, are almost unchanged from the case  $I_v = 0$ . At larger values of  $I_v$ , the phase boundaries change, but we continue to observe the symmetry switching transition from (IIS, ES) to (ES, IIS). Furthermore, as shown in Fig. S4 (b), we continue to observe a hysteresis-like behavior in the range



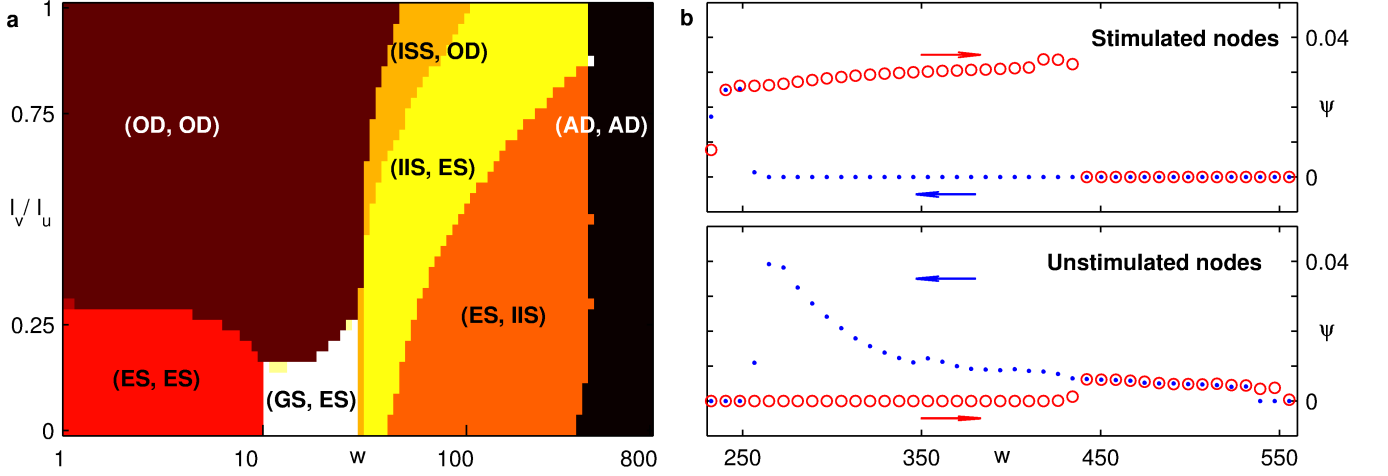


FIG. S4. Collective dynamics of the system on changing model parameters, viz., halving the internal coupling strengths  $c_{\mu,\nu}$ , show results qualitatively similar to those described in the main text. (a) Collective dynamics of a system of  $N = 4$  globally coupled nodes, with  $N_{\text{stim}} = 2$ , showing the different synchronization states obtained by varying the coupling strength  $w$  and the ratio of the input stimuli received by the inhibitory and excitatory components  $I_v/I_u$  (fixing  $I_u = 1.25$ ). (b) Variation of the order parameter  $\psi = \langle \sigma_i^2(v_i) \rangle$  with  $w$  for a network with  $N = 40$ ,  $N_{\text{stim}} = 20$  ( $I_u = 1.25$ ,  $I_v = 0$ ). The behavior of the (top) stimulated and (bottom) unstimulated groups are shown separately. The distinct trends seen on increasing (red circle) or decreasing (blue dots)  $w$  indicate the occurrence of hysteresis-like behavior.

of coupling strengths around the symmetry-switching transition even at large system sizes ( $N = 40$ ,  $N_{\text{stim}} = 20$ ). These observations suggest that the results reported in the main text are robust with respect to small variations in the parameter values and system size.

## NUMERICAL SIMULATIONS

The equations corresponding to the system of  $N$  globally coupled nodes are solved numerically using the variable order method for stiff differential equations as implemented in the `ode15s` routine in MATLAB<sup>®</sup>. The time-series data used for analysis is recorded after allowing sufficient time for any transient effects to dissipate (typically  $2 \times 10^4$  time units).